

## Supporting Information

### Comparing the Energy and Climate Impacts of Conventional Lithium-ion and All-Solid-State Batteries

Zhu Zhu<sup>1</sup>, Rebecca E. Ciez<sup>1,2,\*</sup>

1. School of Sustainability Engineering and Environmental Engineering, Purdue University, West Lafayette, Indiana, 47907, United States

2. School of Mechanical Engineering, Purdue University, West Lafayette, Indiana 47907, United States

\* [rciez@purdue.edu](mailto:rciez@purdue.edu)

Number of Page: 26

Number of Table: 12

Number of Text: 2

#### Table of Contents:

Table S1. Detailed summary of fuel economy (FE) of 2026 all-electric vehicles.

Table S2. Summary of modeled cell-level physical and electrical parameters for LIB and ASSB.

Table S3. Components for one conventional LIB and ASSB cell.

Table S4. Bill of materials for one conventional LIB and ASSB cell.

Table S5. Material inputs for 1 g of NMC811.

Table S6. Unit energy consumption and GHG emission factors for the inputs of NMC811.

Table S7. Unit energy consumption and GHG emission factors for other inputs of both battery cells.

Table S8. Electricity consumption for each manufacturing step of a LIB cell.

Table S9. Electricity consumption of each step for ASSB manufacturing.

Table S10. Embedded energy and GHG emissions of recycling inputs and recovered materials for LIBs

Table S11. Embedded energy and GHG emissions of recycling inputs and recovered materials for ASSBs

Table S12. Comparison with other conventional LIB LCA studies

Text S1. The hydrometrical recycling process for LIBs.

Text S2. The recycling process for ASSBs.

Table S1. Detailed summary of fuel economy (FE) of 2026 all-electric vehicles.

Model	FE	Model	FE
2026 Acura ZDX RWD	0.37	2026 Acura ZDX AWD	0.38
2026 Acura ZDX AWD Type S	0.41	2026 Audi Q4 45 e-tron	0.29
2026 BMW i5 eDrive40 Sedan (19 inch Wheels)	0.31	2026 BMW i5 eDrive40 Sedan (20 inch Wheels)	0.32
2026 BMW i5 eDrive40 Sedan (21 inch Wheels)	0.34	2026 BMW i5 xDrive40 Sedan (19 inch Wheels)	0.34
2026 BMW i5 xDrive40 Sedan (20 inch Wheels)	0.35	2026 BMW i5 xDrive40 Sedan (21 inch Wheels)	0.37
2026 BMW iX xDrive45 (20 inch Wheels)	0.36	2026 BMW iX xDrive45 (21 inch Wheels)	0.38
2026 BMW iX xDrive45 (22 inch Wheels)	0.40	2026 BMW iX xDrive45 (23 inch Wheels)	0.39
2026 BMW iX xDrive60 (20 inch Wheels)	0.35	2026 BMW iX xDrive60 (21 inch Wheels)	0.37
2026 BMW iX xDrive60 (22 inch Wheels)	0.39	2026 BMW iX xDrive60 (23 inch Wheels)	0.40
2026 BMW iX M70 (21 inch Wheels)	0.42	2026 BMW iX M70 (22 inch Wheels)	0.44
2026 BMW iX M70 (23 inch Wheels)	0.45	2026 BMW i7 eDrive50 Sedan (19 inch Wheels)	0.38
2026 BMW i7 eDrive50 Sedan (20 inch Wheels)	0.40	2026 BMW i7 eDrive50 Sedan (21 inch Wheels)	0.39
2026 BMW i7 M70 xDrive Sedan (20 inch Wheels)	0.45	2026 BMW i7 M70 xDrive Sedan (21 inch Wheels)	0.42
2026 BMW i7 xDrive60 Sedan (19 inch Wheels)	0.38	2026 BMW i7 xDrive60 Sedan (20 inch Wheels)	0.41
2026 BMW i7 xDrive60 Sedan (21 inch Wheels)	0.39	2026 Bugatti Rimac Nevera R	0.66

2026 Cadillac LYRIQ (11 kW Charger)	0.37	2026 Cadillac LYRIQ (19 kW Charger)	0.37
2026 Cadillac LYRIQ PAWD V SERIES (11 kW Charger)	0.42	2026 Cadillac LYRIQ PAWD V SERIES (19 kW Charger)	0.42
2026 Cadillac LYRIQ PAWD	0.38	2026 Cadillac VISTIQ (11 kW Charger)	0.39
2026 Cadillac VISTIQ (19 kW Charger)	0.39	2026 Cadillac LYRIQ AWD	0.40
2026 Cadillac OPTIQ RWD (11 kW Charger)	0.32	2026 Cadillac OPTIQ RWD (19 kW Charger)	0.32
2026 Cadillac OPTIQ AWD (11 kW Charger)	0.34	2026 Cadillac OPTIQ AWD (19 kW Charger)	0.34
2026 Cadillac OPTIQ AWD V SERIES 11 kW Charger 15 modes	0.37	2026 Cadillac OPTIQ AWD V SERIES 19 kW charger 15 modes	0.41
2026 Chevrolet Silverado EV 20-mod battery, 19kW 6-mode charger	0.48	2026 Chevrolet Silverado EV 24-mod battery, 19kW 6-mode charger	0.49
2026 Chevrolet Silverado EV 20-mod battery, 11kW 15-mode charger	0.50	2026 Chevrolet Silverado EV 20-mod battery, 19kW 15-mode charger	0.52
2026 Chevrolet Silverado EV 14-mod battery, 11kW 6-mode charger	0.50	2026 Chevrolet Silverado EV 14-mod battery, 11kW 15-mode charger	0.50
2026 Chevrolet Blazer EV FWD	0.32	2026 Chevrolet Blazer EV FWD 22 inch tire	0.36
2026 Chevrolet Blazer EV AWD	0.36	2026 Chevrolet Equinox EV FWD	0.31
2026 Chevrolet Blazer EV AWD SS	0.40	2026 Chevrolet Equinox EV AWD (11 kW Charger)	0.33
2026 Chevrolet Equinox EV AWD (19 kW Charger)	0.35	2026 Dodge Charger Daytona R/T AWD 305/35ZR20	0.39
2026 Dodge Charger Daytona Scat Pack AWD 305/35ZR20	0.39	2026 Dodge Charger Daytona Scat Pack AWD 325/35ZR20 Rear	0.47
2026 Dodge Charger Daytona Scat Pack AWD 325/35ZR20 Rear A/S	0.43	2026 Dodge Charger Daytona R/T AWD 245/55ZR18	0.40
2026 Dodge Charger Daytona R/T AWD 255/45R20	0.36	2026 Dodge Charger Daytona R/T AWD 275/40R20	0.41
2026 GMC Sierra EV 20-mod battery, 11kW 15-mode charger	0.50	2026 GMC Sierra EV 20-mod battery, 19kW 15-mode charger	0.52
2026 GMC Sierra EV 14-mod battery, 11kW 15-mode charger	0.50	2026 Genesis Electrified G80	0.35
2026 Genesis GV60 RWD	0.31	2026 Genesis GV60 AWD (19 inch Wheels)	0.34
2026 Genesis GV60 AWD Advanced (20 inch Wheels)	0.35	2026 Genesis GV60 AWD Performance	0.37
2026 Genesis Electrified GV70 AWD (19 inch Wheels)	0.35	2026 Genesis Electrified GV70 AWD (20 inch Wheels)	0.38
2026 Hyundai Ioniq 9 RWD	0.37	2026 Hyundai Ioniq 9 AWD	0.38
2026 Hyundai Ioniq 9 AWD Performance	0.40	2026 Hyundai Ioniq 5 RWD	0.30

2026 Hyundai Ioniq 5 Standard range	0.29	2026 Hyundai Ioniq 5 AWD (19inch Wheels)	0.32
2026 Hyundai Ioniq 5 AWD (20inch Wheels)	0.34	2026 Hyundai Ioniq 5 AWD XRT	0.36
2026 Hyundai Ioniq 5 N	0.43	2026 Hyundai Ioniq 5 Robo taxi	0.48
2026 Kia Niro Electric	0.30	2026 Kia EV9 Standard Range RWD	0.38
2026 Kia EV9 Long Range RWD	0.38	2026 Kia EV9 Long Range AWD	0.40
2026 Kia EV9 Long Range AWD GT-Line	0.41	2026 Kia EV9 GT	0.43
2026 Lucid Gravity GT w/20F21R wheels (2R)	0.31	2026 Lucid Gravity GT w/21F22R wheels (2R)	0.34
2026 Lucid Gravity GT w/22F23R wheels (2R)	0.34	2026 Lucid Gravity GT w/21F22R wheels (3R)	0.36
2026 Lucid Gravity GT w/22F23R wheels (3R)	0.36	2026 Lucid Gravity Dream w/20F21R wheels (3R)	0.34
2026 Lucid Gravity Dream w/21F22R wheels (3R)	0.38	2026 Lucid Gravity Dream w/22F23R wheels (3R)	0.38
2026 Lucid Air G Touring XR AWD with 19 inch wheels	0.26	2026 Lucid Air G Touring XR AWD with 20 inch wheels	0.28
2026 Lucid Air G Touring XR AWD with 21 inch wheels	0.30	2026 Lucid Air Pure RWD with 19 inch wheels	0.23
2026 Lucid Air Pure RWD with 20 inch wheels	0.26	2026 Lucid Air Sapphire AWD	0.32
2026 Lucid Air Touring AWD with 19 inch wheels	0.25	2026 Lucid Air Touring AWD with 20 inch wheels	0.27
2026 Lucid Gravity GT w/20F21R wheels (3R)	0.32	2026 Mercedes-Benz AMG EQE 4matic Plus	0.48
2026 Mercedes-Benz EQE 320 Plus	0.36	2026 Mercedes-Benz EQE 320 4matic	0.39
2026 Mercedes-Benz EQS 450 Plus	0.34	2026 Mercedes-Benz EQS 580 4matic	0.36
2026 Mercedes-Benz EQS 450 4matic	0.37	2026 Mercedes-Benz EQE 320 Plus (SUV)	0.36
2026 Mercedes-Benz EQE 320 4matic (SUV)	0.42	2026 Mercedes-Benz AMG EQE 4matic Plus (SUV)	0.46
2026 Mercedes-Benz G 580 with EQ Technology	0.54	2026 Mercedes-Benz EQS 400 4matic (SUV)	0.43
2026 Mercedes-Benz EQS 550 4matic (SUV)	0.42	2026 Mercedes-Benz EQS 680 4matic Maybach (SUV)	0.40
2026 Mercedes-Benz CLA250 Plus with EQ Tech	0.31	2026 Mercedes-Benz CLA250 Plus with EQ Tech (R22)	0.27
2026 Mercedes-Benz CLA350 4matic with EQ Tech	0.29	2026 Nissan LEAF 75kWh (18 inch alloy Wheels)	0.30
2026 Nissan LEAF 75kWh (18 inch steel Wheels)	0.28	2026 Nissan LEAF 75kWh (19 inch Wheels)	0.33

2026 Polestar 4 Long Range Single Motor	0.35	2026 Polestar 4 Long Range Dual Motor	0.40
2026 Polestar 4 Long Range Dual Motor Performance	0.44	2026 Rivian R1T Dual Standard (22in)	0.40
2026 Rivian R1T Dual Standard (20in)	0.43	2026 Rivian R1T Dual Max (20in)	0.42
2026 Rivian R1T Dual Max (22in)	0.39	2026 Rivian R1T All-Terrain Dual Max (20in)	0.43
2026 Rivian R1T Performance Dual Max (20in)	0.42	2026 Rivian R1T Performance Dual Max (22in)	0.39
2026 Rivian R1T All-Terrain Performance Dual Max (20in)	0.43	2026 Rivian R1T Dual Large Plus (22in)	0.41
2026 Rivian R1T All-Terrain Dual Large Plus (20in)	0.47	2026 Rivian R1T Performance Dual Large Plus (22in)	0.41
2026 Rivian R1T All-Terrain Performance Dual Large Plus (20in)	0.47	2026 Rivian R1T Dual Large Plus (20in)	0.43
2026 Rivian R1T Performance Dual Large Plus (20in)	0.43	2026 Rivian R1T Tri Max (22in)	0.45
2026 Rivian R1T All-Terrain Tri Max (20in)	0.50	2026 Rivian R1T Dual Large (22in)	0.39
2026 Rivian R1T Dual Large (20in)	0.43	2026 Rivian R1T All-Terrain Dual Large (20in)	0.44
2026 Rivian R1T Performance Dual Large (22in)	0.39	2026 Rivian R1T Performance Dual Large (20in)	0.43
2026 Rivian R1T All-Terrain Performance Dual Large (20in)	0.44	2026 Rivian R1T Quad Max (22in UHP)	0.47
2026 Rivian R1T Quad Max (20in AT)	0.50	2026 Rivian R1T Quad Max (22in)	0.44
2026 Rivian R1S Dual Standard (22in)	0.40	2026 Rivian R1S Dual Standard (20in)	0.43
2026 Rivian R1S Dual Max (20in)	0.42	2026 Rivian R1S Dual Max (22in)	0.40
2026 Rivian R1S All-Terrain Dual Max (20in)	0.43	2026 Rivian R1S Performance Dual Max (20in)	0.42
2026 Rivian R1S Performance Dual Max (22in)	0.40	2026 Rivian R1S All-Terrain Performance Dual Max (20in)	0.43
2026 Rivian R1S Dual Large Plus (22in)	0.41	2026 Rivian R1S All-Terrain Dual Large Plus (20in)	0.47
2026 Rivian R1S Performance Dual Large Plus (22in)	0.41	2026 Rivian R1S All-Terrain Performance Dual Large Plus (20in)	0.47
2026 Rivian R1S Dual Large Plus (20in)	0.43	2026 Rivian R1S Performance Dual Large Plus (20in)	0.43
2026 Rivian R1S Tri Max (22in)	0.45	2026 Rivian R1S All-Terrain Tri Max (20in)	0.50
2026 Rivian R1S Dual Large (22in)	0.39	2026 Rivian R1S Dual Large (20in)	0.43
2026 Rivian R1S All-Terrain Dual Large (20in)	0.44	2026 Rivian R1S Performance Dual Large (22in)	0.39

2026 Rivian R1S Performance Dual Large (20in)	0.43	2026 Rivian R1S All-Terrain Performance Dual Large (20in)	0.44
2026 Rivian R1S Quad Max (22in UHP)	0.47	2026 Rivian R1S Quad Max (20in AT)	0.50
2026 Rivian R1S Quad Max (22in)	0.44	2026 Rolls-Royce Spectre Black Badge (22 inch Wheels)	0.45
2026 Rolls-Royce Spectre Black Badge (23 inch Wheels)	0.48	2026 Rolls-Royce Spectre (22 inch Wheels)	0.44
2026 Rolls-Royce Spectre (23 inch Wheels)	0.48	2026 Subaru Solterra 20 AWD	0.29
2026 Subaru Solterra AWD	0.28	2026 Tesla Model S	0.27
2026 Tesla Model S Plaid	0.31	2026 Tesla Model Y Long Range RWD	0.25
2026 Tesla Model Y Long Range AWD	0.27	2026 Tesla Model X	0.32
2026 Tesla Model X Plaid	0.34	2026 Tesla Model 3 Performance	0.30
2026 Tesla Model 3 Premium AWD	0.26	2026 Tesla Model 3 Premium RWD	0.25
2026 Tesla Cybertruck AWD	0.43	2026 Tesla Model Y Standard RWD (18in Wheels)	0.24
2026 Tesla Model Y Standard RWD (19in Wheels)	0.26	2026 Toyota bZ (energy capacity 200 Ah)	0.26
2026 Toyota bZ LIMITED (energy capacity 200 Ah)	0.27	2026 Toyota bZ AWD	0.28
2026 Toyota bZ AWD LIMITED	0.29	2026 Toyota bZ (energy capacity 191 Ah)	0.26
2026 Toyota bZ LIMITED (energy capacity 191 Ah)	0.27	2026 Volkswagen ID.4	0.30
2026 Volkswagen ID.4 AWD	0.33	2026 Volkswagen ID. Buzz	0.41
2026 Volkswagen ID. Buzz 4motion	0.42	2026 Volvo EX40	0.32
2026 Volvo EC40	0.32	2026 Volvo EX40 Twin	0.36
2026 Volvo EC40 Twin	0.35	2026 Volvo EX30 Single motor extended range	0.29
2026 Volvo EX30 Cross Country (18 Inch Wheels)	0.38	2026 Volvo EX30 Cross Country (19 Inch Wheels)	0.34
2026 Volvo EX30 Twin Performance	0.31		

Note:

I. The unit of fuel economy is kWh/mile.

Table S2. Summary of modeled cell-level physical and electrical parameters for LIB and ASSB.

Parameters	LIB	ASSB
Cell Mass (kg)	0.74 to 0.79	0.56 to 0.58
Cell Volume (L)	0.39 to 0.41	0.32
Nominal Capacity (Ah)	66.90 to 66.92	67.46 to 67.59
Average Voltage (V)	3.71 to 3.75	3.83 to 3.86
Nominal Energy (Wh)	250	250
Upper Cut-Off Voltage (V)	4.25 to 4.8	4.37 to 4.87
Lower Cut-Off Voltage (V)	3.00	3.00

Table S3. Components for one conventional LIB and ASSB cell.

<b>Conventional LIB</b>			
	<b>Base</b>	<b>Low</b>	<b>High</b>
Total Positive Electrode Coating (g)	326.36	297.06	326.36
<i>Positive Active Material(g)</i>	<i>313.30</i>	<i>285.18</i>	<i>313.30</i>
<i>Conductive Additive for Positive Electrode (g)</i>	<i>6.53</i>	<i>5.94</i>	<i>6.53</i>
<i>Positive Electrode Binder (g)</i>	<i>6.53</i>	<i>5.94</i>	<i>6.53</i>
Positive Binder Solvent (g)	104.48	95.04	104.48
Total Negative Electrode Coating (g)	216.56	216.56	216.72
<i>Negative Active Material(g)</i>	<i>212.23</i>	<i>212.23</i>	<i>212.38</i>
<i>Negative Electrode Binder (g)</i>	<i>4.33</i>	<i>4.33</i>	<i>4.33</i>
Positive Foil (g)	32.1	29.3	32.1
Negative Foil (g)	74.9	68.6	74.9
Separator (g)	10.6	9.6	10.6
Electrolyte (g)	89.6	85.4	89.6
Positive Terminal (g)	5.9	5.8	5.9
Negative Terminal (g)	13	12.8	13
Cell Container (PET-Al-PP) (g)	17.26	16.64	17.26
<b>ASSB</b>			
	<b>Base</b>	<b>Low</b>	<b>High</b>
Total Positive Electrode Coating (g)	329.61	299.55	329.61
<i>Positive Active Material(g)</i>	<i>316.42</i>	<i>287.56</i>	<i>316.42</i>
<i>Conductive Additive for Positive Electrode (g)</i>	<i>6.59</i>	<i>5.99</i>	<i>6.59</i>
<i>Positive Electrode Binder (g)</i>	<i>6.59</i>	<i>5.99</i>	<i>6.59</i>
Total Negative Electrode Coating (g)	19.62	19.6	19.62
<i>Negative Active Material(g)</i>	<i>19.62</i>	<i>19.6</i>	<i>19.62</i>
Positive Foil (g)	36.6	36.6	37.6
Negative Foil (g)	85.3	85.3	87.4
Separator (Solid Electrolyte) (g)	78.8	78.8	80.6

Positive Terminal (g)	5.3	5.2	5.3
Negative Terminal (g)	11.7	11.6	11.7
Cell Container (PET-Al-PP) (g)	14.13	13.73	14.13

Note:

I. The italicized text under each cell indicates the specific constituents that make up that cell component.

Table S4. Bill of materials for one conventional LIB and ASSB cell.

<b>Conventional LIB</b>			
	<b>Base</b>	<b>Low</b>	<b>High</b>
NMC811 (g)	313.3	285.18	313.3
Carbon Black (g)	6.53	5.94	6.53
PVDF (g)	6.53	5.94	6.53
NMP (g)	104.48	95.04	104.48
Graphite (g)	212.23	212.23	212.38
Generic Aqueous (g)	4.33	4.33	4.33
Al in Positive Foil (g)	38	35.1	38
Cu (g)	87.9	81.4	87.9
PP/PE/PP (g)	10.6	9.6	10.6
LiPF <sub>6</sub> (g)	13.67	12.94	13.67
EC/DC <sup>I</sup> (g)	75.93	72.46	75.93
	<i>EC (g)</i>	<i>43.74</i>	<i>41.74</i>
	<i>DC (g)</i>	<i>32.19</i>	<i>30.72</i>
PET-Al-PP <sup>II</sup> (g)	17.26	16.64	17.26
	<i>PET (g)</i>	<i>3.70</i>	<i>3.56</i>
	<i>Al (g)</i>	<i>3.38</i>	<i>3.38</i>
	<i>PP (g)</i>	<i>10.18</i>	<i>10.18</i>
<b>ASSB</b>			
	<b>Base</b>	<b>Low</b>	<b>High</b>
NMC811 (g)	316.42	287.56	316.42
Carbon Black (g)	6.59	5.99	6.59
PVDF (g)	6.59	5.99	6.59
NMP (g)	105.44	95.84	105.44
Li (g)	19.62	19.6	19.62
Al in Positive Foil (g)	41.9	41.9	42.8
Cu (g)	97	97	99

Li <sub>3</sub> PS <sub>4</sub> (g)		78.8	78.8	80.6
PET-Al-PP (g)		14.13	13.73	14.13
	<i>PET (g)</i>	<i>3.02</i>	<i>2.94</i>	<i>3.02</i>
	<i>Al (g)</i>	<i>2.77</i>	<i>2.69</i>	<i>2.77</i>
	<i>PP (g)</i>	<i>8.34</i>	<i>8.10</i>	<i>8.34</i>

**Note:**

I. EC refers to Ethylene Carbonate, and DC refers to Diethyl Carbonate. In this study, an EC:DC mixture with a 1:1 volume ratio is assumed.<sup>1</sup>

II. The thickness (equivalently, volume) ratios of the three materials are assumed to be 1:0.47:4.12.<sup>2</sup>

III. The italicized text under each cell indicates the specific constituents that make up that cell component.

Table S5. Material inputs for 1 g of NMC811.

Inputs	Unit	Value	Source
NiSO <sub>4</sub>	g	1.27	GREET <sup>3</sup>
CoSO <sub>4</sub>	g	0.16	
MnSO <sub>4</sub>	g	0.15	
NaOH	g	0.84	
NH <sub>4</sub> OH	g	0.12	
LiOH	g	0.25	
Natural Gas	Wh	11.85	
Electricity	Wh	8.01	

**Note:**

I. NMC811 was synthesized from NiSO<sub>4</sub>, CoSO<sub>4</sub>, and MnSO<sub>4</sub> precursors via co-precipitation using NaOH and NH<sub>4</sub>OH, followed by calcination with LiOH.

Table S6. Unit energy consumption and GHG emission factors for the inputs of NMC811.

Energy Consumption						
	Unit	Base	Low	High	Distribution	Source
NiSO <sub>4</sub>	Wh/g material	24.80	20.10	36.80	Triangular	GREET <sup>3</sup>
CoSO <sub>4</sub>	Wh/g material	28.70			Point Estimate	
MnSO <sub>4</sub>	Wh/g material	2.41			Point Estimate	
NaOH	Wh/g material	8.97			Point Estimate	
NH <sub>4</sub> OH	Wh/g material	17.89			Point Estimate	
LiOH	Wh/g material		39.04	91.08	Uniform	
Natural Gas	Wh/Wh	1.00			Point Estimate	
Electricity	Wh/Wh	1.00			Point Estimate	
GHG Emissions						
	Unit	Base	Low	High	Distribution	Source
NiSO <sub>4</sub>	g CO <sub>2</sub> e/g material	5.02	4.69	10.1	Triangular	GREET <sup>3</sup>
CoSO <sub>4</sub>	g CO <sub>2</sub> e/g material	6.59			Point Estimate	
MnSO <sub>4</sub>	g CO <sub>2</sub> e/g material	0.81			Point Estimate	
NaOH	g CO <sub>2</sub> e/g material	1.95			Point Estimate	
NH <sub>4</sub> OH	g CO <sub>2</sub> e/g material	1.13			Point Estimate	
LiOH	g CO <sub>2</sub> e/g material		12.39	26.84	Uniform	
Natural Gas	g CO <sub>2</sub> e/Wh	0.2458	0.2446	0.2774	Triangular	
Electricity	g CO <sub>2</sub> e/Wh	0.3589	0.0009	0.8713	Triangular	NREL <sup>4</sup>

Table S7. Unit energy consumption and GHG emission factors for other inputs of both battery cells.

Energy Consumption						
	Unit	Base	Low	High	Distribution	Source
Carbon Black	Wh/g material	22.57	15.33	22.95	Triangular	Reference <sup>5</sup>
PVDF		9.82			Point Estimate	GREET <sup>3</sup>
NMP		27.23			Point Estimate	
Graphite			27.20	27.78	Uniform	
Generic Aqueous		12.34			Point Estimate	
Al		32.95	4.50	60.70	Triangular	
Cu		16.15	10.16	18.60	Triangular	
PP/PE/PP		20.98			Point Estimate	
LiPF <sub>6</sub>		47.80			Point Estimate	
EC		2.58			Point Estimate	
DC		10.34			Point Estimate	
PET		20.67			Point Estimate	
Li		68.15			Point Estimate	
Li <sub>3</sub> PS <sub>4</sub>		29.41			Point Estimate	Reference <sup>6</sup>
GHG Emissions						
	Unit	Base	Low	High	Distribution	Source
Carbon Black	g CO <sub>2</sub> e/g material	2.85	1.45	3.50	Triangular	Reference <sup>5</sup>
PVDF		2.12			Point Estimate	GREET <sup>3</sup>
NMP		4.87			Point Estimate	
Graphite			7.82	8.87	Uniform	
Generic Aqueous		3.21			Point Estimate	
Al		7.80	0.97	14.52	Triangular	
Cu		3.89	2.21	4.52	Triangular	

PP/PE/PP		1.79			Point Estimate	
LiPF <sub>6</sub>		9.84			Point Estimate	
EC		0.35			Point Estimate	
DC		1.32			Point Estimate	
PET		2.28			Point Estimate	
Li		19.31			Point Estimate	
Li <sub>3</sub> PS <sub>4</sub>		29.98			Point Estimate	Reference <sup>6</sup>

Table S8. Electricity consumption for each manufacturing step of a LIB cell.

Manufacturing Steps	Unit	Base	Low	High	Distribution
Positive Materials Preparation/Mixing	Wh	280.45	256.49	280.45	Triangular
Negative Materials Preparation/Mixing		320.40	320.40	320.61	Triangular
Positive Electrode Coating		1148.95	1047.08	1148.95	Triangular
Negative Electrode Coating		456.47	431.84	456.47	Triangular
Positive Material Calendering		36.59	33.46	36.59	Triangular
Negative Material Calendering		14.22	13.02	14.22	Triangular
Positive Material Notching		65.05	59.49	65.05	Triangular
Negative Material Notching		69.08	63.24	69.08	Triangular
Vacuum Drying of Positive Electrodes		105.84	97.71	105.84	Triangular
Vacuum Drying of Negative Electrodes		89.51	82.71	89.51	Triangular
Electrode Slitting		69.10	63.22	69.10	Triangular
Cell Stacking		197.02			Point Estimate
Current Collector Welding		73.88			Point Estimate
X-ray Inspection of Cells		16.42			Point Estimate
Inserting Cell in Container		41.05			Point Estimate
Electrolyte Filling and Cell Sealing		98.51			Point Estimate
Dry Room and Dry Room Control System		1,183.27	1167.70	1,183.27	Triangular
Formation Cycling		2954.95			Point Estimate

Table S9. Electricity consumption of each step for ASSB manufacturing.

Manufacturing Step	Electricity Consumption	Source
Production of Li Foil <sup>I</sup>	0.00522 Wh/Anode Area (mm <sup>2</sup> )	Reference <sup>7</sup>
Positive Electrode Preparation/Mixing <sup>II</sup>	4.16 Wh/NMC811 Volume (cm <sup>3</sup> )	Reference <sup>8</sup>
Solid Electrolyte Preparation/Mixing	4.16 Wh/Li <sub>3</sub> PS <sub>4</sub> Volume (cm <sup>3</sup> )	
Positive Electrode Coating <sup>III</sup>	5.55 Wh/Cathode Length (mm)	
Solid Electrolyte Coating	5.55 Wh/Electrolyte Length (mm)	
Positive Electrode and Electrolyte Calendering <sup>IV</sup>	0.177 Wh/ Electrolyte Length (mm)	
Positive Electrode and Electrolyte Slitting <sup>V</sup>	0.166 Wh/Electrolyte Length (mm)	
Negative Electrode Notching <sup>VI</sup>	0.331 Wh/Electrode Length (mm)	
Positive Electrode/Electrolyte Notching <sup>VII</sup>	0.314 Wh/Electrode Length (mm)	
Stacking <sup>VIII</sup>	197 Wh/Cell	
Pressing	3 Wh/Cell	Reference <sup>6</sup>
Welding	74 Wh/Cell	Reference <sup>8</sup>
X-Ray Inspection	16 Wh/Cell	
Inserting Cell in Container	41 Wh/Cell	
Dry Room and Dry Room Control System <sup>IX</sup>	0.0250 Wh/m <sup>2</sup>	
Formation Cycling	2954.95 Wh/Cell	

**Note:**

I. Energy for Li foil production estimated from thermal evaporation (22.75 m<sup>2</sup> h<sup>-1</sup>, 118.7 kW).<sup>7</sup>

II. Cathode and electrolyte mixing energy scaled by volume relative to LIB cathode mixing.<sup>9</sup>

III. Cathode and electrolyte coating energy scaled by length relative to LIB cathode coating.<sup>9</sup>

IV. Cathode and electrolyte calendering energy scaled by length relative to LIB calendaring.<sup>9</sup>

V. Cathode–electrolyte slitting energy scaled by length relative to LIB electrode slitting.<sup>9</sup>

VI. Anode notching energy scaled by length relative to LIB negative electrode slitting.<sup>9</sup>

VII. Cathode–electrolyte notching energy scaled by length relative to LIB positive electrode slitting.<sup>9</sup>

VIII. Stacking, welding, inspection, inserting, and formation cycling are assumed to have the same per-cell energy consumption as LIBs.<sup>9</sup>

IX. The ASSB factory area is assumed to be 105,900 m<sup>2</sup>, calculated as the sum of the areas required for each process, with each process assumed to occupy the same space as its counterpart in LIB manufacturing.

Table S10. Embodied energy and GHG emissions of recycling inputs and recovered materials for LIBs

Embodied Energy						
	Unit	Base	Low	High	Distribution	Source
HCl	Wh/g material	8.725			Point Estimate	GREET <sup>3</sup>
H <sub>2</sub> O <sub>2</sub>		4.721			Point Estimate	
NaOH		8.971			Point Estimate	
Na <sub>2</sub> CO <sub>3</sub>		1.644			Point Estimate	
Al		32.95	4.5	60.7	Triangular	
Cu		16.15	10.16	18.6	Triangular	
Co(OH) <sub>2</sub>		47.884			Point Estimate	
Ni(OH) <sub>2</sub>			0.96	58.4	Uniform	
Mn(OH) <sub>2</sub>		4.092			Point Estimate	
Li <sub>2</sub> CO <sub>3</sub>		21.32	8.87	60.6	Triangular	
GHG Emissions						
HCl	g CO <sub>2</sub> e/g material	1.773			Point Estimate	GREET <sup>3</sup>
H <sub>2</sub> O <sub>2</sub>		0.952			Point Estimate	
NaOH		1.830			Point Estimate	
Na <sub>2</sub> CO <sub>3</sub>		0.681			Point Estimate	
Al		7.8	0.97	14.52	Triangular	
Cu		3.89	2.21	4.52	Triangular	
Co(OH) <sub>2</sub>		11			Point Estimate	
Ni(OH) <sub>2</sub>			0.23	14.43	Uniform	
Mn(OH) <sub>2</sub>		1.38			Point Estimate	

Li <sub>2</sub> CO <sub>3</sub>		8.42	2.81	20.2	Triangular	
---------------------------------	--	------	------	------	------------	--

Table S11. Embodied energy and GHG emissions of recycling inputs and recovered materials for ASSBs

Embodied Energy						
	Unit	Base	Low	High	Distribution	Source
DME	Wh/g material	19.79			Point Estimate	Ecoinvent <sup>10</sup>
FeCl <sub>3</sub>		4.83			Point Estimate	
NMF		36.446			Point Estimate	
Na <sub>2</sub> CO <sub>3</sub>		1.644			Point Estimate	GREET <sup>3</sup>
EtOH		12.96	11.24	19.17	Triangular	
HCl		8.725			Point Estimate	
H <sub>2</sub> O <sub>2</sub>		4.721			Point Estimate	
NaOH		8.971			Point Estimate	
Al		32.95	4.5	60.7	Triangular	
Cu		16.15	10.16	18.6	Triangular	
Co(OH) <sub>2</sub>		47.884			Point Estimate	
Ni(OH) <sub>2</sub>			0.96	58.4	Uniform	
Mn(OH) <sub>2</sub>		4.092			Point Estimate	
Li <sub>2</sub> CO <sub>3</sub>		21.32	8.87	60.6	Triangular	
Li <sub>3</sub> PS <sub>4</sub>		29.41			Point Estimate	Reference <sup>6</sup>
GHG Emissions						
	Unit	Base	Low	High	Distribution	Source
DME	g CO <sub>2</sub> e/g material	2.12			Point Estimate	Ecoinvent <sup>10</sup>
FeCl <sub>3</sub>		1.033			Point Estimate	

NMF		4.0088			Point Estimate	GREET <sup>3</sup>
Na <sub>2</sub> CO <sub>3</sub>		0.6812			Point Estimate	
EtOH		0.1465	0.1362	0.4526	Triangular	
HCl		1.773			Point Estimate	
H <sub>2</sub> O <sub>2</sub>		0.952			Point Estimate	
NaOH		1.830			Point Estimate	
Al		7.8	0.97	14.52	Triangular	
Cu		3.89	2.21	4.52	Triangular	
Co(OH) <sub>2</sub>		11			Point Estimate	
Ni(OH) <sub>2</sub>			0.23	14.43	Uniform	
Mn(OH) <sub>2</sub>		1.38			Point Estimate	
Li <sub>2</sub> CO <sub>3</sub>		8.42	2.81	20.2	Triangular	
Li <sub>3</sub> PS <sub>4</sub>		29.98			Point Estimate	

Table S12. Comparison with other conventional LIB LCA studies

Reference	Cathode-Anode Specific Energy	Energy Consumption (kWh) and GHG Emissions (kg CO <sub>2</sub> e) per kWh of Battery			
		Material Extraction	Manufacturing	EOl Recycling	Recovered Materials
Ciez and Whitacre <sup>11</sup>	NMC622-G	71 kWh	50 kWh	-6 kWh (recycling minus recovered)	
	270 Wh/kg	21 kg	14 kg	-1 kg (recycling minus recovered)	
Kim et al. <sup>12</sup>	NMC-G	NA	NA	NA	NA
	80 Wh/kg	27 kg	62 kg	NA	NA
da Silva Lima et al. <sup>13</sup>	NMC-G	314 kWh	97 kWh	NA	NA
	73 Wh/kg	87 kg	24 kg	NA	NA
Sun et al. <sup>14</sup>	NMC622-G	305 kWh	38 kWh	-44 kWh (recycling minus recovered)	
	115 Wh/kg	105 kg	19 kg	-31 kg (recycling minus recovered)	
Thomas et al. <sup>15</sup>	NMC442-G	NA	NA	NA	NA
	68 Wh/kg	55 kg	9 kg	NA	NA
Kallitsis et al. <sup>16</sup>	NMC111-G	NA	NA	NA	NA
	105 Wh/kg	105 kg	157 kg	NA	NA
Kallitsis et al. <sup>16</sup>	NMC111-GS	NA	NA	NA	NA
	162 Wh/kg	78 kg	102 kg	NA	NA
Kallitsis et al. <sup>16</sup>	NMC622-GS	NA	NA	NA	NA
	182 Wh/kg	71 kg	90 kg	NA	NA
Kallitsis et al. <sup>16</sup>	NMC811-GS	NA	NA	NA	NA
	209 Wh/kg	61 kg	79 kg	NA	NA
Dai et al. <sup>17</sup>	NMC111-G	253 kWh	61 kWh	NA	NA
	143 Wh/kg	59 kg	14 kg	NA	NA
Kelly et	NMC111-G	228 kWh	61 kWh	NA	NA

al. <sup>18</sup>	143 Wh/kg	53 kg	14 kg	NA	NA
Ellingsen et al. <sup>19</sup>	NMC-G 110 Wh/kg	NA 65 kg	NA 110 kg	NA	NA
Majeau-Bettez et al. <sup>20</sup>	NMC-G 112 Wh/kg	333 kWh 140 kg	197 kWh 54 kg	NA	NA
Kallitsis et al. <sup>21</sup>	NMC111-G 105 Wh/kg	NA NA	NA NA	NA 13 kg	NA -78 kg
Tao et al. <sup>22</sup>	NMC-G 120 Wh/kg	1281 kWh (materials and manufacturing) 312 kg (materials and manufacturing)		-273 kWh (recycling minus recovered) -64 kg (recycling minus recovered)	
Tao et al. <sup>22</sup>	NMC-G 120 Wh/kg	1281 kWh (materials and manufacturing) 312 kg (materials and manufacturing)		-232 kWh (recycling minus recovered) -54 kg (recycling minus recovered)	
Mohr et al. <sup>23</sup>	NMC111-G 170 Wh/kg	NA 35 kg	NA 33 kg	NA 6 kg	NA -23 kg
Mohr et al. <sup>23</sup>	NMC111-G 170 Wh/kg	NA 35 kg	NA 33 kg	NA 8 kg	NA -29 kg
Quan et al. <sup>24</sup>	NMC-G 142 Wh/kg	NA 88 kg (materials and manufacturing)	NA	NA -9 kg (recycling minus recovered)	NA
Feng et al. <sup>25</sup>	NMC-G 120 Wh/kg	NA 62 kg (materials and manufacturing)	NA	NA -66 kg (recycling minus recovered)	NA
Gutsch and Leker <sup>26</sup>	NMC811-G 281 Wh/kg (cell only)	NA 41 kg	NA 23 kg	NA 4 kg	NA -28 kg
Gutsch and Leker <sup>26</sup>	NMC811-G 281 Wh/kg (cell only)	NA 41 kg	NA 23 kg	NA 4 kg	NA -24 kg
This Study	NMC811-G 190 Wh/kg	155 kWh [142, 171] 40 kg [35, 46]	29 kWh [28, 29] 11 kg [3, 22]	27 kWh [26, 29] 7 kg [6, 9]	-54 kWh [-81, -26] -14 kg [-22, -7]

**Note:**

I. In anode materials, G is short for Graphite, and S is short for Silicon.

Text S1. The hydrometrical recycling process for LIBs.

### **Step 1. Pretreatment**

The pretreatment begins with discharging, whose energy consumption is calculated using the following equation <sup>27</sup>:

$$E_D = C \times OCV_{avg} \times \eta_{cell}$$

where  $E_D$  is the discharging energy (Wh),  $C$  is the cell capacity (Ah),  $OCV_{avg}$  is the average open-circuit voltage (V), and  $\eta_{cell}$  is the cell efficiency (98%). After discharging, the battery cells are automatically disassembled, with an energy consumption of 50 Wh per cell, consistent with the reported 2.0 kWh for a 40-cell NMC622 module.<sup>28</sup>

Once spent cells have been safely discharged and removed from their packs in the disassembly stage, they are fed into comminution units where they are crushed to separate active materials from the aluminum and copper foils. The resulting slurry is subjected to dense-media separation and screening to sort particles by density and size. High-intensity magnetic separation then recovers paramagnetic metal-oxide fragments. Next, electrostatic separation separates conductive copper and aluminum fragments from nonconductive separator plastics. Finally, filtration removes water from the solid concentrates while recycling process water. The energy consumption in each step is sourced from Reference.<sup>29</sup>

## Step 2. Cathode Soaking and Crushing

The crushed cathode mixture is soaked in NMP at 100 °C for one hour to dissolve the PVDF binder and separate the active NMC material from the aluminum foil. The NMP is assumed to be recycled from the manufacturing stage. The energy requirement for heating is estimated using the specific heat capacity method:

$$E_{heating} = \frac{\sum_{i=1}^3 m_i c_i \Delta T}{\eta}$$

where  $E_{heating}$  is the heating energy consumption (Wh);  $m_i$  is the mass of component  $i$  (g);  $c_i$  is the specific heat capacity of component  $i$  (Wh·g<sup>-1</sup>·K<sup>-1</sup>);  $\Delta T$  is the temperature rise (75 K); and  $\eta$  is the thermal efficiency of the heating system (75%). Here,  $i = 1$  refers to NMP,  $i = 2$  refers to the aluminum foil, and  $i = 3$  refers to the NMC811.

The energy required for crushing was calculated using an average grinding energy intensity of 1.28 MJ/kg.<sup>27</sup>

## Step 3. Filtration and Calcination

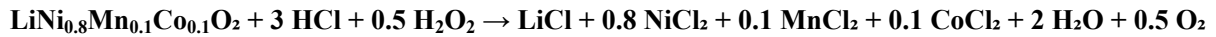
Filtration follows step 2. The energy consumption for filtration is set as 12.73 Wh per cell.<sup>28</sup> The primary purpose of calcination is to remove residual carbon additives, PVDF binder, and the graphite anode material from the recovered black mass fraction. During this step, graphite is oxidized and released as CO<sub>2</sub>, while the NMC cathode material remains in the solid phase. Calcination of cathode material consumes 0.6316 MJ of natural gas and 24.6 Wh of electricity per kg.<sup>11</sup> The CO<sub>2</sub> emissions from the combustion of PVDF and graphite are also included: the complete combustion of 1 g of PVDF produces approximately 1.37 g of CO<sub>2</sub>, while 1 g of graphite yields about 3.66 g of CO<sub>2</sub>.

## Step 4. Grinding

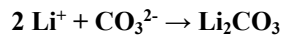
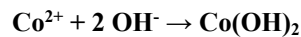
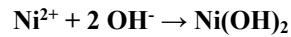
The calcined product was subsequently ground for 2 h, with an energy consumption of 1.28 MJ·kg<sup>-1</sup>.<sup>27</sup>

## Step 5. Leaching and Metal Recovery

Acid leaching uses strong mineral acids (HCl or H<sub>2</sub>SO<sub>4</sub>) to dissolve metal oxides into solution, forming soluble metal salts that can later be recovered. This study uses HCl due to its high dissolution efficiency under mild conditions, as suggested by a previous study.<sup>30</sup> The addition of hydrogen peroxide helps convert high-valent species (Co<sup>3+</sup>, Mn<sup>4+</sup>, Ni<sup>3+</sup>) to their more soluble divalent forms, thereby enhancing both the rate and completeness of metal recovery. This study follows the protocol described in Reference.<sup>30,31</sup> The equation of the leaching reaction is:



Next, filter the reaction mixture to remove any remaining solid material. Finally, Ni, Co, and Mn are sequentially precipitated by adding NaOH: at pH  $\approx$  8, Ni(OH)<sub>2</sub> and Co(OH)<sub>2</sub> co-precipitate; when the pH exceeds 10, Mn(OH)<sub>2</sub> precipitates. The remaining Li<sup>+</sup> is then recovered by precipitating Li<sub>2</sub>CO<sub>3</sub> with Na<sub>2</sub>CO<sub>3</sub>.<sup>31</sup> Filtration follows each precipitation step. The chemical reaction equations are:



In this study, Al and Cu are assumed to have recovery rates of 83%, while Co, Ni, and Mn each reach 98% after leaching and precipitation. Lithium is recovered at 90%.<sup>8</sup> The material inputs for recycling are determined from the corresponding chemical reaction equations. The embedded energy and GHG emissions of both the recycling inputs and recovered materials are summarized in Table S8.

Text S2. The recycling process for ASSBs.

### Step 1. Discharging

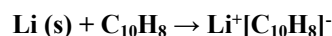
The energy consumption of discharging is calculated using the following equation <sup>27</sup>:

$$E_D = C \times OCV_{avg} \times \eta_{cell}$$

where  $E_D$  is the discharging energy (Wh),  $C$  is the cell capacity (Ah),  $OCV_{avg}$  is the average open-circuit voltage (V), and  $\eta_{cell}$  is the cell efficiency (98%).

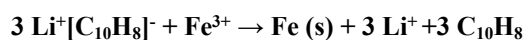
### Step 2. Separating Li-Metal Anode

Metallic lithium was first dissolved in a 1 mol/L naphthalene (Naph) and 1,2-dimethoxyethane (DME) solution, after which filtration separated the Li–Naph solution from the residual black mass. The chemical reaction equation is:



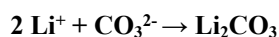
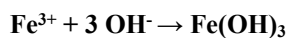
The required amounts of Naph and DME are calculated based on this reaction, while the energy demand for filtration is assumed to be 12.73 Wh.<sup>28</sup>

Excess FeCl<sub>3</sub> was then added, followed by stirring and the introduction of water, producing a reduced Fe precipitate that was removed by filtration. The chemical reaction equation is:



The required amount of FeCl<sub>3</sub> was calculated from this reaction with a 5% excess, while the energy demand for filtration is assumed to be 12.73 Wh.<sup>28</sup>

The resulting filtrate was treated with NaOH to generate a solid Fe by-product, which was collected, and subsequent addition of Na<sub>2</sub>CO<sub>3</sub> yielded a Li<sub>2</sub>CO<sub>3</sub> precipitate that was washed and retained. The chemical reaction equations are:



The required amounts of NaOH and Na<sub>2</sub>CO<sub>3</sub> are calculated based on this reaction, while the energy demand for filtration is assumed to be 12.73 Wh.<sup>28</sup>

Finally, the solvent mixture was recovered by vacuum distillation, with DME distilled at 85 °C and naphthalene at 220 °C. We assume a 95% recovery rate for DME and complete recovery of naphthalene. The energy demand for recovery was calculated based on their specific heat capacities.

### **Step 3. Recovering Solid Electrolyte**

The residual black mass, separated from the Li–Naph solution, was rinsed with DME and subsequently dried at 90 °C to remove residual organic solvents. The DME required for rinsing was assumed to equal the volume of the black mass, with two rinsing steps performed. The energy demand for drying was calculated based on the specific heat capacities.

The dried material was then treated with N-methylformamide (NMF), selectively dissolving Li<sub>3</sub>PS<sub>4</sub> to form a 50 g/L solution, which was subsequently separated by filtration.<sup>32</sup> The filtrate was subjected to controlled solvent evaporation to induce recrystallization of Li<sub>3</sub>PS<sub>4</sub> at 240 °C, which was subsequently collected. A 5% loss of NMF was assumed during recrystallization. The energy consumption of recrystallization is calculated using the specific heat capacity.

### **Step 4. Hydrometallurgical Recycling**

The remaining solid (mainly cathode paste, Al, and Cu) fraction was rinsed with ethanol and dried again at 90 °C. The required amount of ethanol was calculated as twice the volume of the black mass, and the drying energy is calculated using the specific heat capacity.

The remaining solid was separated by comminution, screening, dense media separation, and electrostatic separation. NMC811 was then recovered using the same hydrometallurgical method applied to LIBs.

In this study, Al and Cu are assumed to have recovery rates of 83%, while Co, Ni, and Mn each reach 98% after leaching and precipitation. Li from cathode is recovered at 90%<sup>8</sup> and Li from anode is recovered at 98%. The solid electrolyte is recovered at 98%.

#### Reference:

- 1 S. S. Zhang, T. R. Jow, K. Amine and G. L. Henriksen, *J Power Sources*, 2002, 107, 18–23.
- 2 A. Loukodimou, C. Lovell, G. Theodosopoulos, K. K. Maniam and S. Paul, *Polymers* 2024, Vol. 16, Page 2718, 2024, 16, 2718.
- 3 Argonne National Laboratory, Energy Systems and Infrastructure Assessment, <https://greet.anl.gov/>, (accessed 26 September 2025).
- 4 National Renewable Energy Laboratory, Scenario Viewer | Cambium 2024, <https://scenarioviewer.nrel.gov/?project=a3e2f719-dd5a-4c3e-9bbf-f24fef563f45&layout=Default>, (accessed 26 September 2025).
- 5 F. Rosner, T. Bhagde, D. S. Slaughter, V. Zorba and J. Stokes-Draut, *J Clean Prod*, 2024, 436, 140224.
- 6 A. Keshavarzmohammadian, S. M. Cook and J. B. Milford, *J Clean Prod*, 2018, 202, 770–778.
- 7 M. Burton, S. Narayanan, B. Jagger, L. F. Olbrich, S. Dhir, M. Shibata, M. J. Lain, R. Astbury, N. Butcher, M. Copley, T. Kotaka, Y. Aihara and M. Pasta, *Nat Energy*, 2025, 10, 135–147.
- 8 Argonne National Laboratory, BatPaC: Battery Manufacturing Cost Estimation, <https://www.anl.gov/partnerships/batpac-battery-manufacturing-cost-estimation>, (accessed 19 September 2025).
- 9 Argonne National Laboratory, Battery Performance and Cost Modeling for Electric-Drive Vehicles-A Manual for BatPaC v5.0 , [www.anl.gov](http://www.anl.gov), (accessed 26 September 2025).
- 10 ecoinvent - Data with purpose., <https://ecoinvent.org/>, (accessed 6 October 2025).
- 11 R. E. Ciez and J. F. Whitacre, *Nature Sustainability* 2019 2:2, 2019, 2, 148–156.
- 12 H. C. Kim, T. J. Wallington, R. Arsenault, C. Bae, S. Ahn and J. Lee, *Environ Sci Technol*, 2016, 50, 7715–7722.

- 13 L. da Silva Lima, M. Quartier, A. Buchmayr, D. Sanjuan-Delmás, H. Laget, D. Corbisier, J. Mertens and J. Dewulf, *Sustainable Energy Technologies and Assessments*, 2021, 46, 101286.
- 14 X. Sun, X. Luo, Z. Zhang, F. Meng and J. Yang, *J Clean Prod*, 2020, 273, 123006.
- 15 L. V. Thomas, O. Schmidt, A. Gambhir, S. Few and I. Staffell, *J Energy Storage*, 2020, 28, 101230.
- 16 E. Kallitsis, A. Korre, G. Kelsall, M. Kupfersberger and Z. Nie, *J Clean Prod*, 2020, 254, 120067.
- 17 Q. Dai, J. C. Kelly, L. Gaines and M. Wang, *Batteries 2019, Vol. 5, Page 48*, 2019, 5, 48.
- 18 J. C. Kelly, Q. Dai and M. Wang, *Mitigation and Adaptation Strategies for Global Change 2019 25:3*, 2019, 25, 371–396.
- 19 L. A. W. Ellingsen, G. Majeau-Bettez, B. Singh, A. K. Srivastava, L. O. Valøen and A. H. Strømman, *J Ind Ecol*, 2014, 18, 113–124.
- 20 G. Majeau-Bettez, T. R. Hawkins and A. H. Strømman, *Environ Sci Technol*, 2011, 45, 4548–4554.
- 21 E. Kallitsis, A. Korre and G. H. Kelsall, *J Clean Prod*, 2022, 371, 133636.
- 22 Y. Tao, Z. Wang, B. Wu, Y. Tang and S. Evans, *J Clean Prod*, 2023, 389, 136008.
- 23 M. Mohr, J. F. Peters, M. Baumann and M. Weil, *J Ind Ecol*, 2020, 24, 1310–1322.
- 24 J. Quan, S. Zhao, D. Song, T. Wang, W. He and G. Li, *Science of The Total Environment*, 2022, 819, 153105.
- 25 T. Feng, W. Guo, Q. Li, Z. Meng and W. Liang, *J Energy Storage*, 2022, 52, 104767.
- 26 M. Gutsch and J. Leker, *Appl Energy*, 2024, 353, 122132.
- 27 J. B. Dunn, L. Gaines, M. Barnes, J. L. Sullivan and M. Wang, Material and Energy Flows in the Materials Production, Assembly, and End-of-Life Stages of the Automotive Lithium-Ion Battery Life Cycle, <http://www.osti.gov/servlets/purl/1177517/>, (accessed 26 September 2025).
- 28 M. Choux, S. W. Pripp, F. Kvalnes and M. Hellström, *Resour Conserv Recycl*, 2024, 203, 107430.
- 29 D. Romero Guillén, J. Guimarães Sanches, A. Barbosa Botelho Junior, L. A. Gobo, M. Guimarães Bergerman, D. C. Romano Espinosa and J. A. S. Tenório, *Ind Eng Chem Res*, 2024, 63, 19788–19803.
- 30 W. Xuan, A. Otsuki and A. Chagnes, *RSC Adv*, 2019, 9, 38612–38618.
- 31 H. Wang and B. Friedrich, *Journal of Sustainable Metallurgy*, 2015, 1, 168–178.
- 32 K. Wissel, L. M. Riegger, C. Schneider, A. I. Waidha, T. Famprikis, Y. Ikeda, B. Grabowski, R. E. Dinnebier, B. V. Lotsch, J. Janek, W. Ensinger and O. Clemens, *ACS Appl Energy Mater*, 2023, 6, 7790–7802.